

Two-Dimensional Center-of-Mass Diffusion of Lipid-Tethered Poly(2-methyl-2-oxazoline) at the Air–Water Interface Studied at the Single Molecule Level

Karin Lüdtke,[†] Rainer Jordan,[†] Nathan Furr,[‡] Sumit Garg,[‡] Kelsey Forsythe,[‡] and Christoph A. Naumann^{*·‡}

Wacker-Lehrstuhl für Makromolekulare Chemie, Department Chemie, Technische Universität München, Lichtenbergstrasse 4, 85747 Garching, Germany, and Department of Chemistry, Indiana University–Purdue University Indianapolis, 402 North Blackford Street, Indianapolis, Indiana 46202

Received January 16, 2008. Revised Manuscript Received February 19, 2008

The two-dimensional (2D) center-of-mass diffusion, D , of end-tethered poly(2-methyl-2-oxazoline) (PMOx) lipopolymer chains was studied in a Langmuir monolayer at the air–water interface using wide-field single molecule fluorescence microscopy. In this case, tethering and stabilization of hydrophilic PMOx chains at the air–water interface is accomplished via end-tethering to lipid molecules forming a hydrophobic anchor. To explore the influence of molecular weight, M_n , and surface concentration, c_s , on lateral mobility, two different PMOx chain lengths of $n = 30$ and 50 (n , number of monomer units) were analyzed over a wide range of c_s . Using multiparticle tracking analysis of TRITC-labeled PMOx lipopolymers, we found two regimes of lipopolymer lateral mobility. At low c_s , D is independent of surface concentration but increases with decreasing n . Here diffusion properties are well described by the Rouse model. In contrast, at more elevated c_s , the data do not follow Rouse scaling but are in good agreement with a free area–area model of diffusion. The current study provides for the first time experimental insight into the 2D center-of-mass diffusion of end-tethered polymers at the air–water interface. The obtained results will be of importance for the understanding of diffusion processes in polymer-tethered phospholipid bilayers mimicking biomembranes at low and high tethering concentrations.

Introduction

Soft materials exhibiting two-dimensional (2D) center-of-mass lateral diffusion, D , among their molecular constituents represent an object of great scientific and technological relevance. Prominent examples of such 2D materials are lipid bilayers, copolymers organized into lamellar sheets, wormlike micelles, and ultrathin polymeric films where the film thickness does not notably exceed the hydrodynamic radius of the polymer chains. In such systems, diffusion properties are dependent on multiple factors, including packing density, size and shape of molecules, and molecular interactions.

Among the different types of 2D soft materials, the diffusion properties of amphiphilic phospholipids and diblock copolymers have been explored in particularly great detail. It is now well established that the lateral diffusion of phospholipids in monolayers and bilayers is well described by a two-dimensional form of the free area model.^{1–3} Previous bilayer experiments also showed that the lateral diffusion of lipids in a bilayer geometry can be analyzed using the Rouse concept.⁴ Diblock copolymers, which are organized in lamellar structures, represent another interesting example of a 2D soft material because, unlike phospholipids, they can be studied over a large range of polymer molar masses. Short, unentangled diblock copolymers were found to show Rouse dynamics, whereas diffusion properties of diblocks

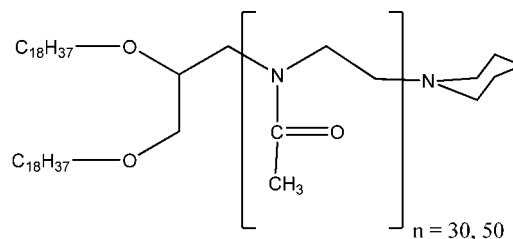


Figure 1. Molecular structures of the lipopolymers diC₁₈PMOx_n ($n = 30, 50$).

of higher molecular weight were interpreted in terms of activated reptation and block retraction, depending on the degree of segregation.^{4–8} Temperature-dependent experiments on polymeric vesicles, which are based on diblock copolymers, also showed that the self-diffusion can be described by a free volume theory.⁴

Here we report on the 2D center of mass diffusion, D , of poly(2-methyl-2-oxazoline) (PMOx) lipopolymers at the air–water interface using wide-field single molecule fluorescence microscopy. This powerful method has been successfully applied before to determine the lateral diffusion of phospholipids in phospholipid and phospholipid/lipolymer monolayers at the air–water interface.^{9,10} In the current study, PMOx lipopolymers of two different polymer chain lengths of $n = 30, 50$ (n , number of monomer units) are compared (Figure 1). Unlike diblock copolymers, which consist of one hydrophilic and one hydro-

* Corresponding author. E-mail: naumann@chem.iupui.edu.

[†] Technische Universität München.

[‡] Indiana University–Purdue University Indianapolis.

(1) Almeida, P. P. F.; Vaz, W. L. C. In *Handbook of Biological Physics, Structure and Dynamics of Membranes Vol. 1A*; Lipowsky, R., Sackmann, E., Eds.; Elsevier: Amsterdam 1995; pp 305–358.

(2) Traeuble, H.; Sackmann, E. *J. Am. Chem. Soc.* **1972**, *94*, 4499–4510.

(3) Galla, H. J.; Hartmann, W.; Theilen, U.; Sackmann, E. *J. Membr. Biol.* **1979**, *48*, 215–236.

(4) Lee, J. C.-M.; Santore, M.; Bates, F. S.; Discher, D. E. *Macromolecules* **2002**, *35*, 323–326.

(5) Dalvi, M. C.; Lodge, T. P. *Macromolecules* **1994**, *27*, 3487–3492.

(6) Ehlich, D.; Takenaka, M.; Hashimoto, T. *Macromolecules* **1993**, *26*, 492–498.

(7) Lodge, T. P.; Dalvi, M. C. *Phys. Rev. Lett.* **1995**, *75*, 657–660.

(8) Hammersky, M. W.; Hillmeyer, M. A.; Tirell, M.; Bates, F. S.; Lodge, T. P. *Macromolecules* **1998**, *31*, 5363–5370.

(9) Ke, P. C.; Naumann, C. A. *Langmuir* **2001**, *17*, 3727–3733.

(10) Ke, P. C.; Naumann, C. A. *Langmuir* **2001**, *17*, 5076–5081.

phobic polymeric block, lipopolymers consist of a hydrophilic polymer chain covalently grafted to a lipid moiety as the headgroup. At the air–water interface, these polymer–lipid hybrids behave like end-tethered polymer chains with mobile grafting points. Consequently, the center of mass diffusion of a lipopolymer monolayer should be confined within the plane of the air–water interface. Because the lipid moiety of lipopolymers, which keeps these amphiphiles at the air–water interface, is usually less spacious than the connected polymer moiety, the self-diffusion properties are expected to be determined mainly by the polymer–polymer interactions. The current experimental system is particularly interesting because the 2D center of mass diffusion can be studied as a function of the surface concentration, c_s . The experiments herein are also important to better understand the diffusion properties of polymer-tethered phospholipid membranes.^{10–17} This is because recent diffusion studies on dye-labeled lipids in polymer-tethered phospholipid monolayers suggest that the lateral diffusion of phospholipids is dependent on the strength of polymer–polymer interactions among adjacent lipopolymers.^{10,18} These findings are in good qualitative agreement with lateral diffusion data of poly(ethylene glycol) (PEG) lipopolymers in magnetically aligned bicelles using NMR, which show two different diffusion regimes at low and high lipopolymer concentrations.^{19,20} In this case, the lateral diffusion of PEG lipopolymers remains largely unchanged in the case of noninteracting or weakly interacting polymer chains but exhibits a significant decrease with increasing strength of interpolymer interaction. Overall, monolayer and bicelle studies suggest an intriguing feedback mechanism between lipid and lipopolymer diffusion in polymer-tethered membranes.

Materials and Methods

The lipopolymers 1,2-di-*O*-*n*-octadecyl-*sn*-glycerol-poly(2-methyl-2-oxazoline)_{*n*} (diC₁₈PMOx_{*n*}) of two different polymer chain lengths of $n = 30, 50$ (n , number of monomer units) were synthesized by living cationic ring-opening polymerization as described recently.^{15,21,22} For each lipopolymer system, a *N*-(6-tetramethylrhodaminethiocarbamoyl) (TRITC)-labeled analogue (diC₁₈PMOx_{*n*}-TRITC, $n = 30, 50$) was created following our previously described strategy.²² The lipopolymers were characterized by gel permeation chromatography, MALDI-TOF mass spectrometry, and ¹H NMR spectroscopy. End-functionalization was quantitative and the polydispersity index (PDI) was found to be narrow with $PDI = M_w/M_n = 1.06$ for diC₁₈PMOx₃₀ and 1.16 for diC₁₈PMOx₅₀. The quantitative dye labeling of a lipopolymer fraction by thiourea coupling was performed as previously reported.²²

To conduct single molecule tracking experiments of amphiphilic lipopolymers at the air–water interface, a custom-built Langmuir trough equipped with a Wilhelmy pressure detector was utilized, as

reported previously.^{9,10} A detailed description of the trough design is provided elsewhere.²³ In short, to allow for imaging experiments using an inverted microscope, the bottom of the Teflon-based trough has an opening at the center, which is sealed by an optically transparent microscopy coverslip (45 × 50 mm). The center of the trough is surrounded by a notably deeper well region to facilitate the immersion of a standalone pressure detector (NIMA) and to enable measurements using a thin water layer in the central area. To avoid water leakage, the precleaned cover glass is slightly pressed against an O-ring using four to six clamps. Prior to the sample being spread, the trough needs to be filled to obtain a water layer of ~5 mm above the cover glass. Lipopolymers were dissolved in chloroform and spread onto the air–water interface, thus forming the lipopolymer monolayer. To facilitate tracking experiments of individual lipopolymers, a small amount of 10^{−8} mol % diC₁₈PMOx_{*n*}-TRITC was added to each monolayer explored, thereby matching n as well as the PDI between labeled and nonlabeled lipopolymers. Milli-Q water (pH = 5.5, 18 MΩ resistivity) was used as the subphase material. After the formation of the monolayer, the monolayer–cover glass distance was reduced to ~200 μm by reducing the subphase volume to suppress the surface flow of the monolayer and to match the 0.25 mm working distance of the 40× water-immersion objective (Olympus UAPO 40× water immersion, NA 1.15) used. To reduce further the perturbation of the monolayer by air flow, the trough was covered and the monolayer was allowed to equilibrate for several minutes prior to imaging. The temperature of the sample cell was maintained at 23.8 °C via a Peltier cooling system (TE Technology).

Our single molecule fluorescence imaging setup was described in more detail previously.^{9,10} A 200 mW frequency doubled Nd:YAG laser (532 nm) was used as an excitation source. The laser beam was spatially filtered and delivered to the EPI port of an inverted microscope (Zeiss Axiovert S100TV). Then the beam was reflected by a dichroic mirror (Omega XF1051) and focused by a microscope objective (Olympus, water immersion, 40× NA = 1.15). The fluorescence signal, centered at 566 nm, was refocused to an intensified CCD camera (iPentaMAX 512EFT, Princeton Instruments) mounted at the TV-port of the microscope. The excitation light was blocked out by the combination of a Raman filter (Omega 540ELP) and the dichroic mirror. To control the exposure time and the time lag between successive exposures, a Uniblitz shutter (VMM-D1) of 3 mm open aperture was utilized. The exposure time and the frame rate of the CCD camera were chosen to be 15 ms and 11 frames/s while synchronized with the Uniblitz shutter.

Image recording and single molecule tracking were acquired using Isee imaging software (Inovision Corp.) running on the Linux platform. The photolability of fluorescent dyes does not allow for long-term observations of individual molecules and a straightforward analysis of the diffusion processes using a mean-square displacement, $\langle r^2 \rangle$, versus time analysis. Therefore, the positional change of individual molecules was analyzed for each successive frame separately using a constant time lag between successive exposures of $t_{\text{tag}} = 50$ ms, as reported before.¹² The time lag was set by the time of closed shutters between successive exposures (open shutters). The exposure time was set to 7 ms. To minimize the impact of surface flow on the experimental results, the relative positional change of multiple tracer molecules was analyzed (multiple particle tracking) by tracking the position of two to four molecules at a given CCD frame and by determining the changing distances among tracer molecules between successive frames. Finally, flow-corrected square displacements, r^2 , were obtained from the relative distance values. To ensure statistical significance, each sample was analyzed using 150 flow-corrected square displacements at the same $t_{\text{tag}} = 50$ ms. The r^2 were first investigated in terms of a cumulative distribution function (CDF) by counting the number of r^2 with values $\leq r^2$ and normalizing by the total number of tracks used.²⁴ Each CDF was analyzed assuming normal diffusion, for which the CDF is²⁴

- (11) Wagner, M. L.; Tamm, L. K. *Biophys. J.* **2000**, *79*, 1400–1414.
 (12) Deverall, M. A.; Gindl, E.; Sinner, E.-K.; Besir, H.; Ruehe, J.; Saxton, M. J.; Naumann, C. A. *Biophys. J.* **2005**, *88*, 1875–1886.
 (13) Tanaka, M.; Sackmann, E. *Nature* **2005**, *437*, 656–663.
 (14) Purucker, O.; Förtig, A.; Jordan, R.; Tanaka, M. *ChemPhysChem* **2004**, *5*, 327–335.
 (15) Purucker, O.; Förtig, A.; Lüdtkke, K.; Jordan, R.; Tanaka, M. *J. Am. Chem. Soc.* **2005**, *127*, 1258–1264.
 (16) Purucker, O.; Grönnewein, S.; Förtig, A.; Jordan, R.; Rusp, M.; Bärmann, M.; Moroder, L.; Sackmann, E.; Tanaka, M. *Soft Matter* **2007**, *3*, 333–336.
 (17) Purucker, O.; Förtig, A.; Jordan, R.; Sackmann, E.; Tanaka, M. *Phys. Rev. Lett.* **2007**, 98078102–1078102–4.
 (18) Naumann, C. A.; Knoll, W.; Frank, C. A. *Biomacromolecules* **2001**, *2*, 1097–1103.
 (19) Soong, R.; Macdonald, P. M. *Biophys. J.* **2005**, *88*, 255–268.
 (20) Soong, R.; Macdonald, P. M. *Biochim. Biophys. Acta* **2007**, *1768*, 1805–1814.
 (21) Jordan, R.; Martin, K.; Räder, H. J.; Unger, K. K. *Macromolecules* **2001**, *34*, 8858–8865.
 (22) Bonnè, T.; Lüdtkke, K.; Jordan, R.; Stepanek, P.; Papadakis, C. M. *Colloid Polym. Sci.* **2004**, *282*, 833–843.

(23) Murcia, M. J.; Garg, S.; Naumann, C. A. In *Methods in Membrane Lipids*; Dopic, A., Ed.; Humana Press: Totowa, NJ, 2007; pp 277–294.

(24) Schuetz, G.; Schindler, H.; Schmidt, T. *Biophys. J.* **1997**, *73*, 1073–1080.

$$P(r^2, t_{\text{lag}}) = 1 - \exp\left(-\frac{r^2(t_{\text{lag}})}{\langle r^2(t_{\text{lag}}) \rangle}\right) \quad (1)$$

where $\langle r^2(t_{\text{lag}}) \rangle$ is the mean-square displacement and t_{lag} is the time lag. In addition, CDFs were analyzed for anomalous subdiffusion, with

$$P(r^2, t) = \gamma(a, br^c) / \Gamma(a) \quad (2)$$

where $\gamma(a, br^c)$ and $\Gamma(a)$ are the incomplete and complete gamma functions and a , b , and c are constants.¹² The mean-square displacement, $\langle r^2 \rangle$, was determined from the flow-corrected square displacements, r^2

$$\langle r^2 \rangle = \frac{1}{\sum_{t_i - t_j = t_{\text{lag}}} \sum_{t_i - t_j = t_{\text{lag}}} [\vec{r}(t_i) - \vec{r}(t_j)]^2} \quad (3)$$

where $\vec{r}(t_i)$ and $\vec{r}(t_j)$ are the position vectors of the tracer molecule at times t_i and t_j , respectively. As reported previously, the statistical conditions (number of r^2 per sample) chosen result in a deviation in $\langle r^2 \rangle$ of 1.5%.¹² For Brownian diffusion, the lateral diffusion coefficient D can be obtained from the average value of the individual displacements $\langle r^2 \rangle$ with

$$D = \frac{\langle r^2 \rangle}{4t_{\text{lag}}} \quad (4)$$

Results and Discussion

Figure 2 shows the pressure (π)–area (A) isotherms of diC₁₈PMOx₃₀ (solid line) and diC₁₈PMOx₅₀ (dashed line) monolayers at the air–water interface. Those regions are marked by arrows, where single molecule imaging studies were conducted. The absence of a plateau at a film pressure of about 10 mN/m, which has been observed for poly(ethylene glycol) (PEG) and poly(2-ethyl-2-oxazoline) lipopolymers having a polymer main chain of slight amphiphilicity, indicates the pure hydrophilic nature of the PMOx chains.^{25–28} As highlighted in the inset of Figure 2, diC₁₈PMOx₃₀ and diC₁₈PMOx₅₀ are both characterized by a plateau at elevated surface concentrations. This plateau region has been associated with a surface micellization, which also has been observed on diblock copolymers.^{4,28,29} Interestingly, the further increase of the lipopolymer surface concentration

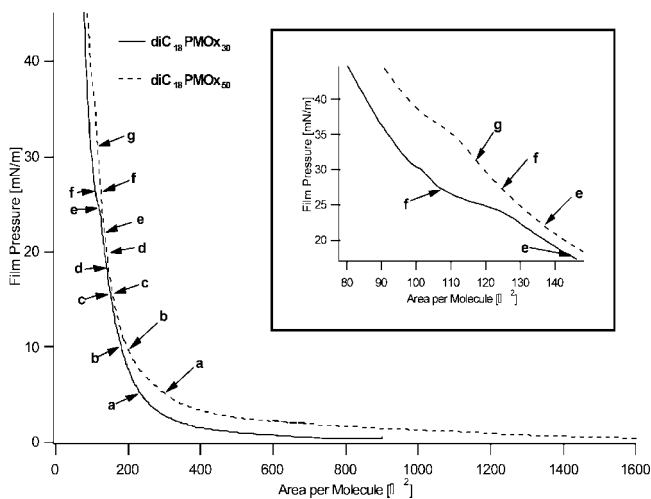


Figure 2. Pressure–area isotherms of diC₁₈PMOx₃₀ and diC₁₈PMOx₅₀. The markers illustrate where single molecule fluorescence microscopy studies were conducted. The inset shows an enlargement of the region around the high-pressure transition, which has been associated with the formation of surface micelles.

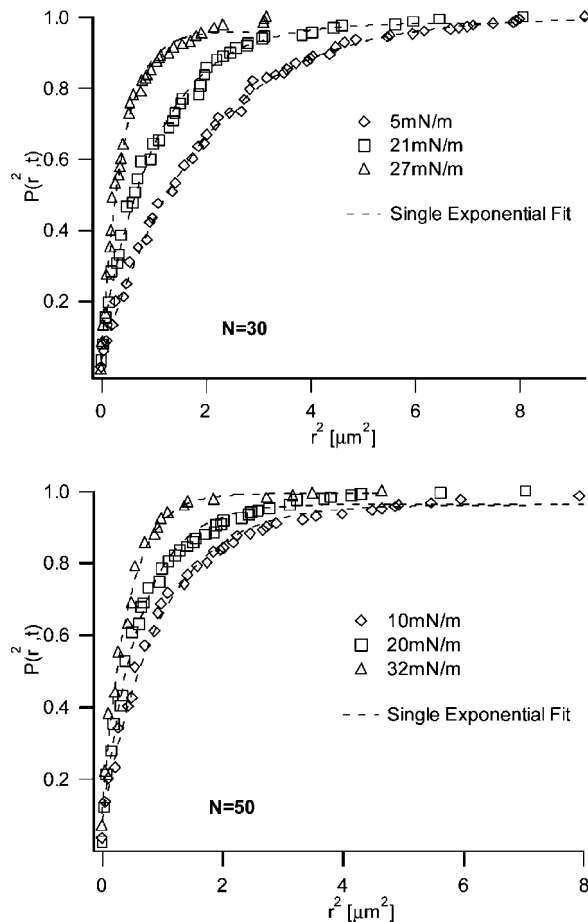


Figure 3. Normalized cumulative distribution function (CDF) obtained from TRITC-labeled PMOx lipopolymers in monolayers of diC₁₈PMOx₃₀ (top) and diC₁₈PMOx₅₀ (bottom). For each lipopolymer system, CDFs are illustrated which were obtained from three representative film pressures. The dashed line shows the best fit using the theoretical CDF describing Brownian diffusion (eq 1). All r^2 are based on a time lag of $t_{\text{lag}} = 50$ ms.

beyond the surface micellization transition leads to a significant change in viscoelastic properties, which has been associated with the jamming of surface micelles.^{28,30} This viscoelastic transition is dependent on the lipid and polymer moieties of these amphiphiles.^{28,31}

The photolability of organic dyes prevents a reliable tracking analysis over a large time range. Therefore, the lateral mobility of probe molecules was examined using CDFs of a constant $t_{\text{lag}} = 50$ ms, as described before.¹² Figure 3 illustrates representative CDFs obtained from tracking experiments at different film pressures using monolayers of diC₁₈PMOx₃₀ and diC₁₈PMOx₅₀. The CDFs show qualitative agreement between the two different lipopolymers ($n = 30, 50$) in that increasing film pressures shift r^2 to smaller values at a given $P(r^2, t)$. This shift, which corresponds to a reduction in lateral mobility, is reasonable due

(25) Baekmark, T. R.; Elender, G.; Lasics, D. D.; Sackmann, E. *Langmuir* **1995**, *11*, 3975–3987.

(26) Baekmark, T. R.; Wiesenthal, T.; Kuhn, P.; Bayerl, T. M.; Nuyken, O.; Merkel, R. *Langmuir* **1999**, *15*, 3616–3626.

(27) Lüdtke, K.; Jordan, R.; Hommes, P.; Nuyken, O.; Naumann, C. A. *Macromol. Biosci.* **2005**, *5*, 384–393.

(28) Foreman, M. B.; Coffman, J. P.; Murcia, M.; Cesana, S.; Jordan, R.; Smith, G. S.; Naumann, C. A. *Langmuir* **2003**, *19*, 326–332.

(29) Baekmark, T. R.; Sprenger, I.; Ruile, M.; Nuyken, O.; Merkel, R. *Langmuir* **1998**, *14*, 4222–4226.

(30) Naumann, C. A.; Brooks, C. F.; Fuller, G. G.; Knoll, W.; Frank, C. W. *Langmuir* **1999**, *15*, 7752–7761.

(31) Coffman, J. P.; Naumann, C. A. *Macromolecules* **2002**, *35*, 1835–1839.

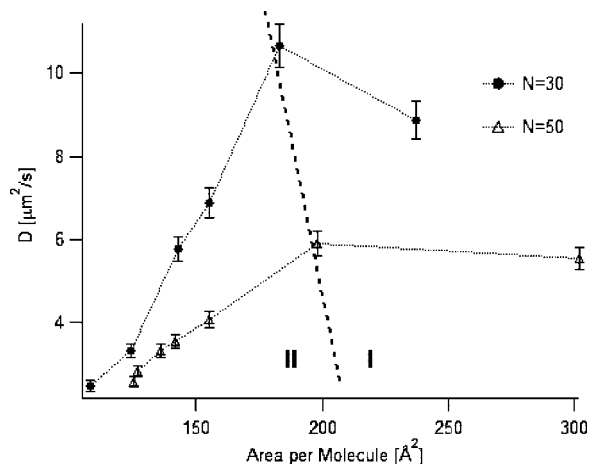


Figure 4. Diffusion coefficient, D , plotted as a function of area per molecule, A , for $\text{diC}_{18}\text{PMOx}_{30}$ and $\text{diC}_{18}\text{PMOx}_{50}$. Each lipopolymer system shows two different diffusion regions, regions I and II. At lower surface concentrations (region I), D appears to be independent of A . In contrast, at more elevated surface concentrations (region II), D gradually decreases with decreasing A . The dotted lines connect the data points to guide the eye.

to the smaller areas per molecule at increased film pressures. Figure 3 also reveals that the experimental CDFs presented can be described quite well by eq 1 representing the theoretical CDF for Brownian diffusion (dashed lines). In fact, the fits did not improve notably if the theoretical model considering anomalous diffusion (eq 2) was applied (data not shown). The excellent agreement between experimental and theoretical CDFs based on the Brownian diffusion model suggests that the multiple-particle tracking analysis approach employed successfully corrected for surface flow and that D can be determined from $\langle r^2 \rangle$ using eq 4. The current results do not exclude the possibility of anomalous subdiffusion at longer time lags. Unfortunately, a more rigorous analysis of anomalous subdiffusion is not possible in the current study because the poor photostability of fluorescent dyes prevents the $\langle r^2 \rangle$ -time analysis over a wide range of different time lags. It should be pointed out that anomalous diffusion was reported on nonentangled polymer fluids.³²

To further analyze the diffusion behavior of lipopolymers at the air–water interface, Figure 4 illustrates plots of D versus the area per molecule, A , for both lipopolymers studied. Several interesting results can be obtained. Unlike phospholipids at the air–water interface,⁹ lipopolymers exhibit two different diffusion regimes labeled as regions I and II, which are dependent on the surface concentration, c_s . In region I, at high area per molecule, A , D is independent of A and the average plateau value of D increases with decreasing n . Beyond a critical area per molecule, A_{crit} , in region II, D decreases with decreasing A . Here the slope of the D - A plots is dependent on n . Interestingly, the tracking results in Figure 4 show great similarities to the concentration-dependent diffusion of bulk polymers where two similar diffusion regions have been observed.^{33–35} In this case, the polymer diffusion at the plateau region is well-described by the Rouse model, whereas the diffusion data at more elevated concentrations are in good agreement with the concept of reptating polymer chains.

To interpret the tracking data in Figure 4, one needs to consider the lipid–polymer hybrid character of lipopolymers. The hybrid character gives rise to two possible diffusion mechanisms. The first mechanism emphasizes on the fact that lipopolymers in a planar geometry mainly interact via their polymeric moiety. In this case, the analysis within the framework of polymer diffusion theory seems to be justified. In contrast, the second mechanism treats lipopolymers as regular amphiphiles like phospholipids without particularly considering the polymeric nature of their hydrophilic moiety. The main rationale for such an interpretation is that polymer chains are end-tethered to lipids, thus confining them at the air–water interface, and are relatively short with no or minor entanglements. Here the lateral diffusion should be well described by a free-area model. In the following, we want to interpret our tracking data in terms of these two concepts.

The plateau region of region I suggests Rouse diffusion. In the Rouse regime, the self-diffusion coefficient, D , and the polymer molecular weight, M_n , of bulk polymers are related via³⁶

$$D \propto M_n^{-1} \quad (5)$$

The tracking data of the two lipopolymers ($n = 30, 50$) in the plateau region reveal the following ratio

$$\frac{D_{1,30}}{D_{1,50}} = \frac{9.7}{5.7} = 1.7$$

Here $D_{1,30}$ and $D_{1,50}$ are the D values of $\text{diC}_{18}\text{PMOx}_{30}$ and $\text{diC}_{18}\text{PMOx}_{50}$, respectively, in region I. Indeed, this ratio agrees well with the corresponding ratio based on the Rouse prediction of eq 5, which can be expressed by

$$\frac{D_{\text{diC}_{18}\text{PMOx}_{30}}}{D_{\text{diC}_{18}\text{PMOx}_{50}}} = 50/30 = 1.67$$

The above finding is in good agreement with previous reports on other 2D soft materials, where Rouse diffusion was observed as well. For example short, unentangled diblock copolymers and phospholipids which are organized in vesicular structures, show Rouse-type diffusion properties.⁴ Rouse diffusion was also observed on another interesting 2D soft material, DNA bound to planar lipid bilayers containing cationic lipids.³⁷

In region II, at more elevated c_s , the lipopolymer diffusivity is characterized by enhanced polymer–polymer interactions. Because D is now dependent on c_s and cannot be described by eq 5, the tracking results cannot be explained in terms of simple Rouse dynamics anymore. At the same time, it is not plausible to interpret the diffusion properties of lipopolymers in region II in terms of a chain reptation process, where the self-diffusion of reptating polymers in bulk can be expressed by $D \propto c^{-\alpha} M_n^{-\beta}$ (c , bulk concentration; D , diffusion coefficient) with scaling exponents of $\alpha = 1.75$ and $\beta = 2$.^{33,38} This is because the relatively short polymer chains are end-tethered to lipids, thus confining them at the air–water interface. To verify our assumption, Figure 5 illustrates the tracking data related to region II in terms of $\log D$ - $\log c_s$ plots for both systems studied. Interestingly, $\text{diC}_{18}\text{PMOx}_{30}$ and $\text{diC}_{18}\text{PMOx}_{50}$ are characterized by different values of α , which are $\alpha = 4.9$ for $\text{diC}_{18}\text{PMOx}_{30}$ and $\alpha = 2.4$ for $\text{diC}_{18}\text{PMOx}_{50}$. Furthermore, these scaling exponents significantly deviate from that of reptating polymers in bulk ($\alpha = 1.75$). Figure 5 also provides information about the

(32) Guenza, M. *Macromolecules* **2002**, *35*, 2714–2722.

(33) Léger, L.; Hervet, H.; Rondelez, F. *Macromolecules* **1981**, *14*, 1732–1738.

(34) Smith, D. E.; Perkins, T. T.; Chu, S. *Phys. Rev. Lett.* **1995**, *75*, 4146–4149.

(35) Kaes, J.; Strey, H.; Sackmann, E. *Nature* **1994**, *368*, 226–229.

(36) Doi, M.; Edwards, S. F. *The Theory of Polymer Dynamics*; Clarendon Press: Oxford, 1988.

(37) Maier, B.; Raedler, J. O. *Phys. Rev. Lett.* **1999**, *82*, 1911–1914.

(38) de Gennes, P. G. *J. Chem. Phys.* **1971**, *55*, 572–579.

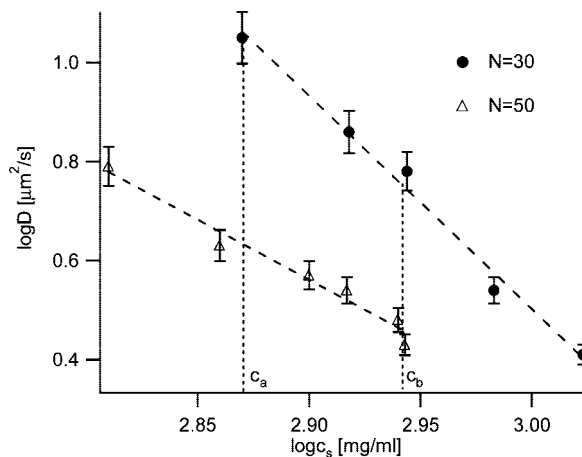


Figure 5. log–log plot of the diffusion coefficient D vs surface concentration c_s of diC₁₈PMOx₃₀ and diC₁₈PMOx₅₀ in diffusion region II. The dashed lines represent linear fits to the data, their slopes change with n and are -4.9 ($n = 30$) and -2.4 ($n = 50$). The overlap region is highlighted by c_a and c_b , respectively.

scaling exponent β . This is achieved by analyzing the overlap region of diC₁₈PMOx₃₀ and diC₁₈PMOx₅₀ between c_a and c_b . Here, the scaling exponent β (averaged over the whole overlap region) was found to be $\beta = 1.6 \pm 0.3$. Overall, the scaling exponents α and β obtained from Figure 5 show, as expected, that chain reptation is not the appropriate model to describe the diffusion data in region II.

Because the water molecules are expected to remain inside the polymer system due to hydrodynamic interactions (nondraining behavior), it is reasonable to assume that the diffusion process can be described in terms of a rigid body model, like a free-area model, where polymers can be approximated via circular disks, spheres, or cylinders.^{39–41} The free area model has the general form⁴²

$$D = D_0 \exp\left(-\frac{\gamma a}{a_f} - \frac{E_a}{kT}\right) \quad (6)$$

where D_0 is the diffusion coefficient describing free diffusion, a^* is a critical free area, a_f is the average free area, E_a is an activation energy, k is the Boltzmann constant, and T is the temperature. The activation energy takes into account the interactions between amphiphiles, the interactions between amphiphiles and solvent molecules, and the required energy for the formation of free area.^{43,44} A limiting form of eq 6 without the energy term was developed earlier by Cohen and Turnbull.⁴⁵ By applying the limiting case of Cohen and Turnbull to our monolayer system, we can write

$$D = D_0 \exp\left(-\frac{\gamma A_{\min}}{A_f}\right) \quad (7)$$

where A_{\min} is the minimum free area per lipopolymer required for diffusion and A_f is the average free area per lipopolymer

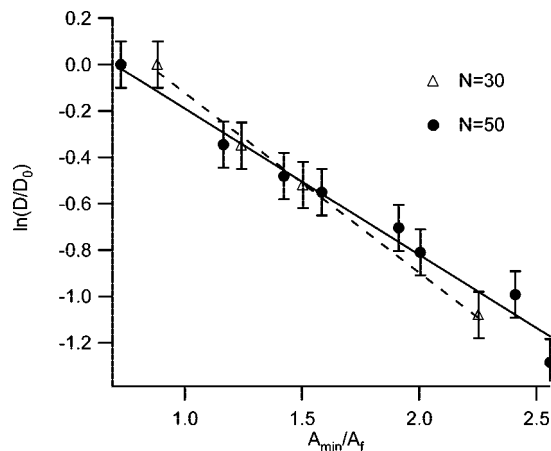


Figure 6. Plot of $\ln(D/D_0)$ vs A_{\min}/A_f for $n = 30, 50$ in diffusion region II. The dashed and solid lines represent the best linear fits for $n = 30$ and $n = 50$, respectively. Their slopes are -0.77 ($n = 30$) and -0.66 ($n = 50$). The excellent agreement between data points and fits shows that D of end-tethered PMOx chains in diffusion region II is well described by the free area model.

which is given by $A_f = A_{\text{lipo}} - A_{\min}$. A hallmark of the free-area model is that there is a linear relationship between $\ln D$ and the inverse of the free area, $1/A_f$. To explore the free area concept in more detail, Figure 6 illustrates $\ln(D/D_0)$ vs A_{\min}/A_f plots for diC₁₈PMOx₃₀ and diC₁₈PMOx₅₀ in diffusion region II. Here A_{\min} was estimated for each lipopolymer by extrapolating the D vs A plot toward $D = 0$ (not shown). The dashed and solid lines represent the best linear fits of the tracking data using eq 7 for $n = 30$ and $n = 50$, respectively. The excellent agreement between linear fits and data points shows that the diffusion properties of diC₁₈PMOx₃₀ and diC₁₈PMOx₅₀ are well-described by the free-area model. Furthermore, the determined γ -values of $\gamma = 0.77$ (diC₁₈PMOx₃₀) and $\gamma = 0.66$ (diC₁₈PMOx₅₀), which can be obtained from the slopes of the plots in Figure 6, are well within the expected range of $0.5 \leq \gamma \leq 1$.¹

Conclusion

The current wide-field single molecule fluorescence microscopy study provides for the first time insight into the 2D center-of-mass diffusion of lipid-tethered poly(2-methyl-2-oxazoline) at the air–water interface. By exploring the diffusion properties of two different polymer chain lengths over a wide range of surface concentrations, we were able to investigate the influence of the polymer chain length and molecular surface concentration on the 2D center-of-mass diffusion. Depending on surface concentration c_s , our experiments reveal two different diffusion mechanisms. At low c_s , the 2D center-of-mass diffusion shows typical features of a Rouse system. In contrast, at more elevated c_s , where more pronounced interpolymer interactions occur, diffusion properties are better described by a free-area model, at least, in the absence of surface micelles. The experiments presented herein will be of interest for the understanding of diffusion processes in polymer–lipid composites like polymer-tethered phospholipid monolayers and bilayers.^{12,14–17,19,20}

Acknowledgment. Funding for this work was provided by the Petroleum Research Fund (PRF#36751-G7) and the National Science Foundation (MCB-0416779). R.J. gratefully acknowledges funding from the Deutsche Forschungsgemeinschaft via the SFB 563 “*Bioorganic Functional Systems on Solids*” (TP A8-Jordan) as well as through the DFG project JO 287/4-1.

LA8001493

(39) de Gennes, P. G. *Scaling Concepts in Polymer Physics*; Cornell University Press, Ithaca, NY, 1979.

(40) Vianney, J. M.; Koelman, A. *Phys. Rev. Lett.* **1990**, *64*, 1915–1918.

(41) Falck, E.; Punkkinen, O.; Vattulainen, I.; Ala-Nissila, T. *Phys. Rev. E* **2003**, *68*, 050102.

(42) Macedo, P. B.; Litovitz, T. A. *J. Chem. Phys.* **1965**, *42*, 245–256.

(43) Clegg, R. M.; Vaz, W. L. C. In *Progress in Protein-Lipid Interactions*; Watts, A., DePont J. J. H. H. M., Eds.; Elsevier: Amsterdam, 1985; Vol. 1, pp 173–229.

(44) Almeida, P. P. F.; Vaz, W. L. C.; Thompson, T. E. *Biochemistry* **1992**, *31*, 6739–6747.

(45) Cohen, M. H.; Turnbull, D. *J. Chem. Phys.* **1959**, *31*, 1164–1169.